Enhancement of the electro-activated persulfate process in dye removal using graphene oxide nanoparticle

Bita Ayati and Zeinab Ghorbani

ABSTRACT

This study aimed to improve the speed of the electrochemical process by graphene oxide nanoparticle as a current accelerator in Acid Blue 25 removal from aqueous solutions. To do so, the effect of different parameters including pH, dye concentration, sodium persulfate concentration, the ratio of sodium persulfate to iron (II) sulfate concentration, current density, and the distance between electrodes was investigated on dye removal. Under optimal conditions of pH = 5, dye concentration = 200 mg/L, sodium persulfate concentration = 500 mg/L, iron (II) sulfate concentration = 100 mg/L, current density = 16.67 mA/cm^2, and electrode distance = 2 cm, 95% of dye was removed after 60 min in the electro-activated persulfate process; while the modified electro-activated persulfate process achieved 95% dye removal after only 40 min under the same conditions. This system was able to remove 90% of dye after 60 min at a higher concentration (300 mg/L). Also, the modified electro-activated persulfate process obtained the removal of 80% of COD, and 54% of TOC after 180 min in the mentioned conditions, for the dye concentration of 300 mg/L.

Key words | Acid Blue 25, electrochemical process, energy consumption, ferrous ion, graphene oxide nanoparticle

Bita Ayati (corresponding author)
Civil and Environmental Engineering Faculty,
Tarbiat Modares University,
P.O. Box 14115-397,
Tehran,
Iran
E-mail: *ayati_bi@modares.ac.ir*

Zeinab Ghorbani
Civil and Environmental Engineering,
Tarbiat Modares University,
Tehran,
Iran

HIGHLIGHTS

- Geraphene oxide nanoparticles raised the reaction rate by 17% by increasing the conductivity.
- The increase in conductivity, decreased the energy consumption by 50%.
- More 100 mg/L dye can be removed by the modified system.
- The oxidation state reduction made the dye structure simpler with less toxicity.

doi: 10.2166/wst.2021.128

GRAPHICAL ABSTRACT

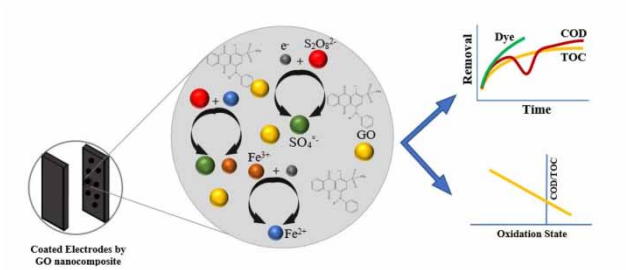

INTRODUCTION

Persulfate ion ($S_2O_8^{2-}$) was first introduced in 1912 by Hugh Marshal. However, its application in the advanced oxidation process as an essential factor in the production of the powerful oxidizing radical ($SO_4^{\bullet-}$) has been overshadowed by the capabilities of hydroxyl radical ($OH^{\bullet}$) produced by hydrogen peroxide (H_2O_2) (Ike *et al.* 2018). The redox potential of persulfate (2.01 V) is among the highest as an oxidizing agent in advanced oxidation processes (Devi *et al.* 2016). Persulfate and the sulfate radical have special and unique properties such as high kinetic velocity and more stability compared to hydroxyl radicals, as well as less dependence on organic matter (which has a higher effect on organic matter) (Kansal *et al.* 2010). However, it has a low oxidation rate at room temperature and in the absence of a catalyst, which can be activated by heat, UV, alkalinity, activated carbon, and metal ions. Activation of persulfate, which involves the breaking of O-O bond, leads to the production of sulfate radicals ($SO_4^{\bullet-}$) with a high oxidizing ability (Zahraa *et al.* 2006). This unstable radical is highly active that rapidly attacks organic matter molecules and separates a hydrogen atom from the structure of organic matter (Robinson *et al.* 2001; Asadi & Mehrvar 2006). The redox potential of sulfate radicals produced by activating persulfate depends on the way of its activation. However, activation of persulfate using Fe^{2+} has been studied many times due to its high removal efficiency and its being non-toxic, environmentally friendly, and cost-effective (Wang & Wang 2018).

In recent years, electrochemical processes as environmentally friendly technology have been widely used in the removal of various pollutants from water and wastewater sources (Yuan *et al.* 2013). Using persulfate along with electrolysis (electro persulfate process), compared to the conventional method of activating persulfate with Fe^{2+}, improves the consumption of persulfate, reduces Fe^{3+} to Fe^{2+}, lowers the amount of sludge and reactor volume, which leads to the reduction of operating costs (Lin *et al.* 2013; Zou *et al.* 2013; Silveira *et al.* 2017; Waclawek *et al.* 2017). Equation (1) shows the reaction of a persulfate ion with an electron released from the electrochemical system that results in the production of sulfate radicals. Also, based on Equation (2), persulfate ion can be regenerated at the cathode, which is called cathodic activation (Liu *et al.* 2018a, 2018b).

$$S_2O_8^{2-} + e^- \rightarrow SO_4^{2-} + SO_4^{\bullet-} \quad (1)$$

$$2SO_4^{2-} \rightarrow S_2O_8^{2-} + 2e^- \quad (2)$$

Many studies have been conducted using the electro-activated persulfate process for the removal of various pollutants. For example, Liu *et al.* (2018a, 2018b) carried out their studies on the reduction of tetracycline hydrochloride by combining the electrochemical oxidation process with persulfate, which removed 81% of 50 mg/L pollutant in 240 min (Liu *et al.* 2018a, 2018b). Cai *et al.* (2018) conducted their research on the electrochemical oxidation of 2 and 4-dichlorophenoxyacetic acid using the electro-activated persulfate process with the highest removal efficiency of 96% at the current density of 5 mA/cm^2 (Cai *et al.* 2018). Li *et al.* (2018) performed their studies on the reduction of 2 and 4-dinitrophenol in aqueous solutions using the electro persulfate process with a ring-shaped anode made of sheet iron, which resulted in the maximum COD removal of 63.4% in 15 min and the concentration of 5 mM persulfate (Li *et al.* 2018).

Graphene is a new type of carbon nanoparticle that can be used to make polymer nanoparticles. Graphene is pure carbon in the form of a thin sheet with a thickness of one atom, which is very strong despite its low weight (almost 100 times stronger than steel). Graphene has a two-

dimensional network with covalent bonds that have attracted much attention due to its unusual physicochemical, electrical and mechanical structure and properties, high specific surface area, good electron transfer and distribution, low cost, and excellent electrical conductivity (Cai *et al.* 2009; Li *et al.* 2009; Zhang *et al.* 2017). Graphene oxide is used as a catalyst, an adsorbent, and an electric current accelerator, which can improve the performance of electrochemical systems and increase the rate of persulfate oxidation (Lu *et al.* 2014). Graphene oxide surface includes a large number of functional groups (carboxyl, hydroxyl, epoxy group, etc.). These special functional groups cause the proper distribution and hydrophobicity of graphene in water, which makes it a suitable option for the production of electrodes that store electrical current. Graphene also improves the electrical conductivity and cycling stability of the electrode (Kim *et al.* 2006; Szabo *et al.* 2006).

In this research, the effect of graphene oxide nanoparticles on increasing the reaction rate and activation of persulfate, the current density and the energy consumed in the electro-persulfate system for removing organic pollutants, especially dyes that are non-degradable has been analyzed. To the best of our knowledge, none of the previous researches investigating the efficiency of nano graphene oxide contained electrodes and adding iron (II) sulfate manually as a catalyst to remove Acid Blue 25. Besides, the electrical consumption of this novel system has been compared to the conventional electro-persulfate system.

MATERIALS AND METHODS

Materials and equipment

The pollutant investigated in this study was Acid Blue 25 (with the chemical formula of $C_{20}H_{13}N_2NaO_5S$ and natural pH = 8.2), which has the anthraquinone structure (containing 1 benzene ring and 1 naphthalene ring) and is widely used in textiles, leather, and paper industries (Idel-aouad *et al.* 2011). Acid Blue 25, from Alvan Sabet Hamedan Company, chemical compounds including sodium hydroxide and sulfuric acid to balance pH, sodium persulfate and iron (II) sulfate for main tests, silver sulfate, mercury sulfate (II), potassium dichromate for COD testing, and sodium sulfate for creating a better current, were purchased from Merck Company. In order to produce graphene oxide nanoparticles, pure graphene was purchased from Siraj Company, and phosphoric acid 96%, hydrochloric acid 30%, hydrogen peroxide, and potassium permanganate were provided from Merck Company.

In this research, the main equipment includes DR/4000 UV-Visible spectrophotometer made by Hach company for analyzing dye degradation, COD reactor made by Hach to prepare samples for COD degradation, UE-6SFD ultrasonic cleaner made by Fungilab for nanoparticle homogenization, MP-3005D power supply made by Megatek for providing electrical current to the system, MIRA3 TESCAN-XMU field emission scanning electron microscopy (FESEM), X'Pert MPD X-ray diffraction (XRD) for surface and morphological analyzing, LiquiTOC II TOC analyzer to evaluate mineralization of organic pollutant, Metrohm digital pH meter (model 691) to adjust and analyze the solution pH, DEM-ERD electric furnace model F.69 for calcination of the compounds, ATF digital steel oven, Mettler PJ300 digital scale (with the accuracy of 0.001 g) for sample weighing, and magnetic stirrer model H5-860 made by Tayfeh Azma Company.

Characterization of graphene oxide

Graphene oxide nanoparticles' surface morphology was analyzed by FESEM, and XRD patterns were obtained to investigate the crystal structure of synthesized nanomaterials.

Methods

The electrochemical reactor used was made of glass with a volume of 500 mL (Figure 1). In all experiments, graphite electrodes (measuring $120 \times 60 \times 120$ mm) were used due to their cost-effectiveness, which were fixed vertically by a metal rod insulated with plastic.

Before conducting each test, both electrodes were purified by acetone and distilled water to remove any contaminants. At each step of the study, the reactor content (synthetic wastewater) was stirred on a magnetic stirrer to make proper contact between the materials, and every 10 min, the samples were taken. In order to eliminate the possible adverse effect of sludge on the results, the samples were centrifuged for 1 min at a speed of 3,000 rpm, and the

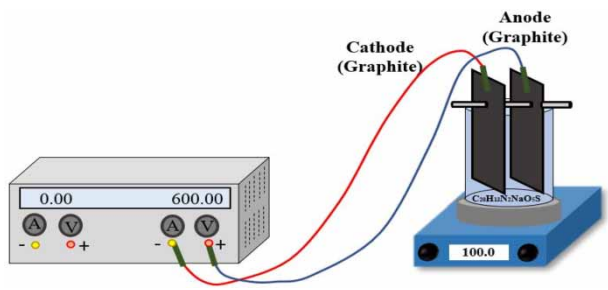

Figure 1 | A scheme of the pilot in this study.

dye concentration was measured at the maximum wavelength (602 nm).

In this study, the one-factor-at-a-time (OFAT) method was used for experiments. So, the parameters were optimized by keeping all parameters constant, except one of them. In this study, the values of parameters were examined according to the following: 3, 5, 6, 7, 8.2, and 11 for pH, 50, 100, 150, 200, and 250 mg/L for dye concentration (common concentration range in textile wastewater (Idel-aouad *et al.* 2011)), 300, 400, 500, and 600 mg/L for sodium persulfate concentration, 50, 100, 150 and 200 mg/L for iron (II) sulfate concentration, 0.357, 0.417, 0.5, 0.625, and 0.833 A for current, and 1, 2, and 3 cm for the distance between the electrodes. In all experiments, the net cross-section of the electrodes was 300 mm^2, the concentration of sodium sulfate was 1,600 mg/L, the stirrer speed was 100 rpm, and the temperature was 24–26 °C. It should be noted that each experiment was repeated three times in all steps to avoid possible errors, and the maximum error was considered 5%.

In electrochemical processes, measuring energy consumption is the basis for estimating economic costs. The amount of energy consumed in this study was calculated using Equation (3) (Nayebi & Ayati 2021). Current density is also one of the most significant parameters in the electrochemical process, which is calculated by Equation (4) (Li *et al.* 2018). The value of the net cross-section of the electrode was considered 30 cm^2, due to its small effect on removal efficiency, and the current was investigated as the main parameter. Also, Equations (5)–(7) show zero, first- and second-order kinetics. The oxidation state value was also calculated, according to Equation (8) (Eckenfelder 1999).

$$E = \frac{VIT}{C - C_0} \tag{3}$$

Where:

E: energy consumed to remove each mg of pollutant (J/mg)
V: potential difference (V)
I: current (A)
T: time (s)
C: secondary concentration (mg/L)
C_0: initial concentration (mg/L)

$$J = \frac{I}{A} \tag{4}$$

Where:

J: current density (A/cm^2)
I: current (A)
A: net cross-section of the electrode (cm^2)

$$C_0 = K_0 t \tag{5}$$

$$LnC_0/C = K_1 t \tag{6}$$

$$1/C - 1/C_0 = K_2 t \tag{7}$$

Where:

K: velocity constant
C_0: initial concentration
C: dye concentration at time t

$$OX = 4(TOC - COD)/TOC \tag{8}$$

Where:

OX: oxidation state
TOC: total organic carbon (mg/L)
COD: chemical oxygen demand (mg/L)

In order to modify the electro-activated persulfate process, graphene oxide nanoparticles were synthesized by the modified Hummers' method (Gholami *et al.* 2017; Zaaba *et al.* 2017); first, sulfuric acid (360 mL) and phosphoric acid (40 mL) were mixed for a few minutes. Then, the graphite powder (3 g) was added to the mixture. Thereafter, the potassium permanganate (18 g) was slowly added to the solution, and the solution was stirred for 6 h to obtain a dark green solution. Afterwards, 3 mL of hydrogen peroxide was slowly added to the solution and was stirred for 10 min to remove excess potassium permanganate. The solution was placed in an ice bath due to the exothermic reactions. Then, hydrochloric acid (10 mL) and deionized water (30 mL) were added to the mixture, and the solid particles were separated by a centrifuge at 5,000 rpm (7 min). The material on the surface was removed, and the remaining solid particles were washed three times with HCl and deionized water. The obtained graphite oxide was then placed in an ultrasonic device to get a brown graphene oxide solution, and in the end, the washed graphene oxide was placed in an oven at 90 °C for 24 h to obtain graphite oxide.

In order to coat graphite electrodes with graphene oxide nanoparticles, the sol-gel method, which is one of the conventional coating methods and has shown good stability, was used. One of the best ways for fixing nanoparticles on graphite electrode is to use polytetrafluoroethylene (PTFE) material as a bonding agent between nanoparticles and the electrode surface. For this purpose, the desired amount of

graphene oxide nanoparticles, Teflon powder (3 times of the weight of nanoparticles), 30 mL distilled water, and 3% volume percent of 1-butanol were placed in an ultrasonic bath for 20 min. The resulting mixture was then heated to 80 °C until oily. Finally, the resulting mixture was poured on the electrode and placed in a furnace for 15 min at 350 °C for calcination (Khataee *et al.* 2013).

Additional experiments were conducted separately, after obtaining the optimal conditions, to investigate other reactions such as COD and TOC removal and the kinetic evaluation. To determine the amount of chemical oxygen consumption, Method 5220 D. Closed Reflux, the Colorimetric method, from 'Standard Methods for the Examination of Water and Wastewater' was used (APHA 2017).

RESULTS AND DISCUSSION

The optimal conditions of the electro-persulfate process on dye removal

In the following, the effect of pH, dye concentration, sodium persulfate concentration, sodium persulfate to iron sulfate (II) ratio, current, and the distance between electrodes was investigated on Acid Blue 25 removal using the electro-activated persulfate process including, and the results is showed in Table 1.

Effect of optimal pH

The most efficient parameter in advanced oxidation and electrochemical processes is the pH of the solution. In advanced oxidation processes using Fe^{2+} to activate $S_2O_8^{2-}$ and produce $SO_4^{\bullet-}$, pH affects the species and the state of iron in solution and the reaction of $S_2O_8^{2-}$ with the contaminant (Rastogi *et al.* 2009). The results of dye removal experiments in a various range of pH are presented in Table 1. As shown in the table, by increasing the pH from 3 to 7, the dye removal efficiency decreases and then increases.

As pH gradually moves from the acidic to the alkaline range, a large amount of the iron is converted to Fe^{3+}, and since only Fe^{2+} can activate $S_2O_8^{2-}$, by reducing the ratio of Fe^{2+} to Fe^{3+}, the removal efficiency significantly decreased. Also, as pH goes above 4, the solubility of Fe^{2+} remaining in the solution reduces, and the iron becomes colloidal. This phenomenon, in turn, reduces efficiency (Masomboon *et al.* 2010). It should be noted that by increasing the pH above 9, ferric oxyhydroxide is produced by reactions 9 and 10, which has too low ability to activate $S_2O_8^{2-}$ (Zhou *et al.* 2013).

$$Fe^{2+} + H_2O \rightarrow FeOH^{+} + H^{+} \quad (9)$$

$$2Fe^{3+} + 2H_2O \rightarrow Fe_2(OH)_2^{4+} + 2H^{+} \quad (10)$$

Fe^{3+} produced based on reactions (11) and (12) is converted to Fe^{2+} again, which according to can use electrons released in the electrochemical system (reaction (13)) and activate $S_2O_8^{2-}$. Also, the released electrons in the system based on reaction (14) can activate persulfate, which leads to an increase in removal efficiency (Li *et al.* 2018).

$$Fe^{2+} + S_2O_8^{2-} \rightarrow Fe^{3+} + SO_4^{\bullet-} + SO_4^{2-} \quad (11)$$

$$Fe^{2+} + SO_4^{\bullet-} \rightarrow Fe^{3+} + SO_4^{2-} \quad (12)$$

$$Fe^{3+} + e^{-} \rightarrow Fe^{2+} \text{ (Cathode)} \quad (13)$$

$$S_2O_8^{2-} + e^{-} \rightarrow SO_4^{\bullet-} + SO_4^{2-} \quad (14)$$

Effect of initial dye concentration

The results of the dye removal test at different initial dye concentrations and energy consumption are presented in Table 1. As shown in the table, the dye removal efficiency after 60 min for dye concentrations of 50, 100, 150, 200, and 250 mg/L is 94.5, 90, 88, 85, and 75%, respectively. According to the results, by increasing the dye concentration, the removal efficiency decreases. The difference in dye removal efficiency at concentrations of 100 and 200 mg/L is small. However, the rate of reduction of removal efficiency at the concentration of 250 mg/L is significant. In general, the dye removal efficiency decreases by increasing initial dye concentration. Because at high concentrations, the production of oxidizing radicals on the surface of the catalyst decreases due to the occupation of active sites by dye molecules, while the number of oxidizing radicals remains constant (Idel-aouad *et al.* 2011). Also, increasing the concentration of pollutants leads to the production of more by-products due to oxidation, which will consume more sulfate radicals (Zazouli & Taghavi 2012). Therefore, the reaction between the catalyst and the oxidizer is disrupted, and the removal efficiency is reduced (Panda *et al.* 2011). A negligible decrease in removal efficiency at concentrations between 100 and 200 mg/L can be explained by the Hassan-Hameed collision theory, according to which the probability of a collision between organic matter and

Table 1 | The optimal conditions of the electro-persulfate process on dye removal

Parameter	Amount	Values of other parameters	Dye removal efficiency (%) After 60 min	Energy consumption in 90% dye removal efficiency	Optimum amount
pH	3	$[Na_2S_2O_8] = 300$ mg/L, [Dye] = 50 mg/L,	93.7	101	5
	5	$[FeSO_4] = 100$ mg/L, I = 0.5 A, d = 3 cm	94.4	101.2	
	6		86.8	118	
	7		70.8	132.4	
	8.2		68.9	145.2	
	9		75	126.9	
	11		79	123.1	
Initial dye concentration (mg/L)	50	$[Na_2S_2O_8] = 300$ mg/L, $[FeSO_4] =$	94.5	100	200
	100	100 mg/L, pH = 5, I = 0.5 A, d = 3 cm	90	55.6	
	150		88	37.2	
	200		85	35.1	
	250		75	31.3	
$[Na_2S_2O_8]$ (mg/L)	300	$[FeSO_4] = 100$ mg/L, pH = 5, I = 0.5 A,	85	35.2	500
	400	[Dye] = 200 mg/L, d = 3 cm	87.5	27.8	
	500		95	19.2	
	600		97	18.5	
$[SO_4^{2-}]/[Fe^{2+}]$	10	$[FeSO_4 = 100$ mg/L, pH = 5, I = 0.5 A,	86	28	5
	5	[Dye] = 200 mg/L, d = 3 cm	95	19	
	3.33		93	21.4	
	2.5		92	24.6	
Current (mA)	357	[Dye] = 200 mg/L, pH = 5, $[Na_2S_2O_8] =$	87	15.14	500
	417	500 mg/L, $[FeSO_4] = 100$ mg/L, d = 3 cm	88.5	18.75	
	500		95	18.5	
	625		93	29.8	
	833		93.5	55.5	
Distance between electrodes (cm)	1	[Dye] = 200 mg/L,pH = 5, $[Na_2S_2O_8] =$	92	15.7	2
	2	500 mg/L, $[FeSO_4] = 100$ mg/L, I = 0.5 A	95.5	16	
	3		95	23.2	

oxidizing species increases by increasing the number of dye molecules per unit volume. This issue will increase the dye removal efficiency or decrease it negligibly (Hassan & Hameed 2011).

According to Table 1, the minimum energy consumption to achieve the desired dye removal efficiency is for the concentration of 200 mg/L. The difference between energy consumption at concentrations of 200 and 250 mg/L is not significant. Nevertheless, since the difference in dye removal efficiency between them is 10%, the concentration of 200 mg/L was chosen as the optimal concentration and was used as a basis in the following experiments.

Effect of sodium persulfate concentration and sodium persulfate to iron (II) sulfate concentration ratio

In order to determine the optimal initial concentration of sodium persulfate and the optimal ratio of sodium persulfate to iron sulfate (II) as the main parameters of this process, the results of the dye removal test at different concentrations of sodium persulfate are presented in Table 1.

As can be seen, the dye removal efficiency after 60 min for the persulfate concentrations of 300, 400, 500, and 600 mg/L is 85, 87.5, 95, and 97%, respectively. There is a positive correlation between the concentration of persulfate and dye removal efficiency. Due to the small difference in dye removal efficiency at concentrations of 500 and 600 mg/L, the concentration of 500 mg/L was selected as the optimal value considering economic issues.

Also, the dye removal efficiency after 60 min for sodium persulfate to iron (II) sulfate concentration ratios of 10, 5, 3.33, and 2.5 is 86, 95, 93, and 92%. It can be seen that by increasing the concentration of iron (II) sulfate from 50 to 100 mg/L, the dye removal efficiency increases and then decreases slightly from 100 to 200 mg/L. Because by adding Fe^{2+} to the reactor, the process is efficient in the

first few minutes, and then by converting Fe^{2+} to Fe^{3+} (reaction (15)), the efficiency of the process stops. Therefore, a high concentration of Fe^{2+} must be added to the solution, which results in the production of a large volume of sludge. Also, according to reaction (16), Fe^{2+} acts as a radical scavenger for persulfate and produces other sulfate species that have low oxidizing power (Jiang *et al.* 2013).

$$Fe^{2+} + S_2O_8^{2-} \rightarrow SO_4^{\bullet -} + SO_4^{2-} + Fe^{3+} \quad (15)$$

$$Fe^{2+} + SO_4^{\bullet -} \rightarrow Fe^{3+} + SO_4^{2-} \quad (16)$$

Therefore, considering the results, the iron (II) sulfate concentration of 100 mg/L, and the sodium persulfate and iron (II) sulfate ratio of 5 were selected as the optimal values.

Effect of electrical current

The results of the dye removal efficiency at different current and energy consumptions at 90% removal efficiency are presented in Table 1, respectively. As can be observed, the dye removal efficiency after 60 min for currents of 357, 417, 500, 625, and 833 mA is 87, 88.5, 95, 93, and 93.5%, respectively. By increasing the current from 357 to 500 mA, the dye removal efficiency increases and then decreases. Also, by increasing the current from 357 to 500 mA, the amount of energy consumption almost remains constant (about 20 kWh/kg). Nonetheless, from the current of 500 to 833 mA, the amount of energy consumption has increased at high speed.

The presence of electricity causes the continuous release of Fe^{2+} into the solution and the activation of persulfate to produce the $SO_4^{\bullet -}$ radical (reaction (15)). More $SO_4^{\bullet -}$ radicals are also produced through electron transfer (Reaction (17)). The main reaction at the cathode is the increase of the production of Fe^{2+} by Fe^{3+} reduction on the cathode surface, which results in the activation of persulfate (reaction (18)). As the current increases, Fe^{2+} accumulates in the solution, and the extra Fe^{2+} acts as a scavenger for $SO_4^{\bullet -}$ and $OH^{\bullet}$ (reactions (19) and (20)) (Lin *et al.* 2014; Li *et al.* 2018).

$$S_2O_8^{2-} + e^- \rightarrow SO_4^{\bullet -} + SO_4^{2-} \quad (17)$$

$$Fe^{3+} + e^- \rightarrow Fe^{2+} \quad \text{(Cathode)} \quad (18)$$

$$Fe^{2+} + SO_4^{\bullet -} \rightarrow SO_4^{2-} + Fe^{3+} \quad (19)$$

$$Fe^{2+} + OH^{\bullet} \rightarrow Fe^{3+} + OH^- \quad (20)$$

When the current passes from a specific amount, the removal efficiency decreases. This might be due to the reactions caused by high current densities and the cathodic evolution of hydrogen gas based on reaction (21), which competes with electrons for sulfate radicals through reaction (20) to obtain electrons (Liu *et al.* 2018a, 2018b).

$$2H^+ + 2e^- \rightarrow H_2 \quad (21)$$

Therefore, considering the description provided, the current of 500 mA was selected as the optimal value. Also, considering the optimal values of the electrode cross-section and current, the optimal current density was 16.67 mA/cm^2 based on Equation (4).

Effect of the distance between electrodes

The results of the dye removal efficiency at different distances of the electrodes and the amount of energy consumed in 90% removal efficiency are also presented in Table 1. As shown in this table, the dye removal efficiency after 60 minutes for the electrode distances of 1, 2, and 3 cm is 92, 95.5, and 95%, respectively. This result might be because at greater distances, the mass transfer of the catalyst particles to the cathode surface is limited, and the reduction of Fe^{2+} on the catalyst surface stops. As a result, the activation of persulfate for producing active radicals is not done properly (Lu *et al.* 2014). Also, according to the energy consumption data, the distance between the electrodes and the energy consumption have a positive correlation. As the distance between the electrodes decreases due to the reduction of the electrical resistance of the system, the voltage required to achieve a constant current decreases and, as a result, the energy consumption decreases. Also, the energy consumption in the small electrode distance (1 cm) is due to the lack of proper transfer of materials and fluids, which leads to the accumulation of solid particles and bubbles between the anode and cathode and increases electrical resistance (Phalakornkule *et al.* 2010). Therefore, considering that the energy consumption in the distance of 3 cm (between 15 and 25 kWh/kg) is more than that at the distance of 2 cm (between 10 and 15 kWh/kg), 2 cm was selected as the optimal value of the distance between electrodes.

Enhancement of electro-activated persulfate process

Due to the unique properties of graphene oxide nanoparticles in accelerating the electric current, this material was used to improve the electro-activated persulfate process.

Evaluation of the characteristics of coated electrodes

Figure 2 shows the FESEM of the graphite electrode surface, before (Figure 2(a)) and after (Figure 2(b)) coating with graphene oxide nanoparticles with a magnification of 75000. As can be seen, the particle size of the coated nanoparticles is between 30 and 70 nm, and due to the magnification of the image, most of the coated particles on the surface are less than 2 nm. Also, the surface of the graphite electrode was layered (Figure 2(b)), which increased the adhesion of graphene oxide nanoparticles to the graphite surface. Other notable points are the relatively uniform coverage and lack of nanoparticle mass formation.

Figure 3 also shows the XRD of the electrode surface after coating with graphene oxide nanoparticles. This image shows the crystal structure of graphene oxide nanoparticles with light refraction peaks with 2θ at 12^0 and 43^0. As can be seen, after the oxidation process on the graphite composition in this diffraction pattern, the sharp peak of graphite at 2θ is very weak at 23.30, which indicates that the graphite composition is converted well to graphene oxide. The sharp and weak peaks in the 2θ region are 12.40 and 41.90, respectively, corresponding to the plates (002) and (100) of the graphene oxide compound. The peak transfer from $2\theta = 23.30$ in the graphite composition to the peak at $2\theta = 12.40$ in the graphene oxide composition is due to the presence of functional groups in the graphite layers, which causes the distance between the layers to increase. The distance between the graphene oxide nanocomposite layers was 0.713 nm. Compared to graphite

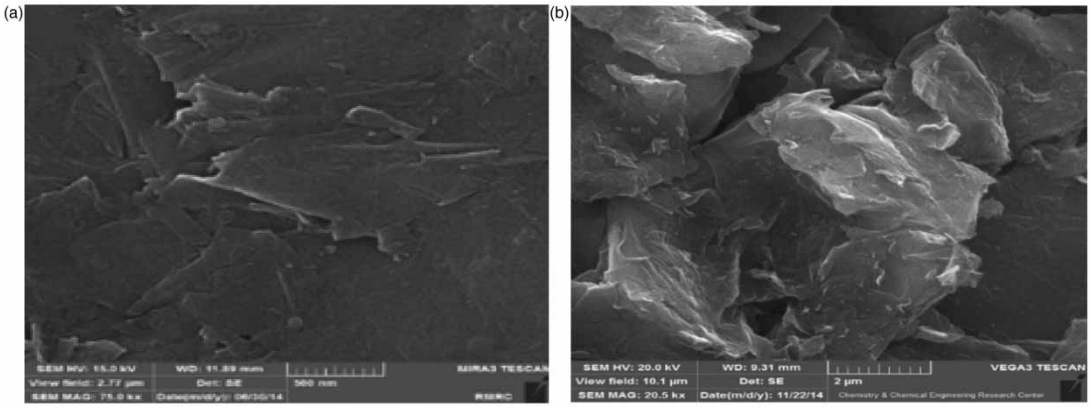

Figure 2 | FESEM (a) graphite electrode (b) graphite electrode coated with graphene oxide nanoparticles.

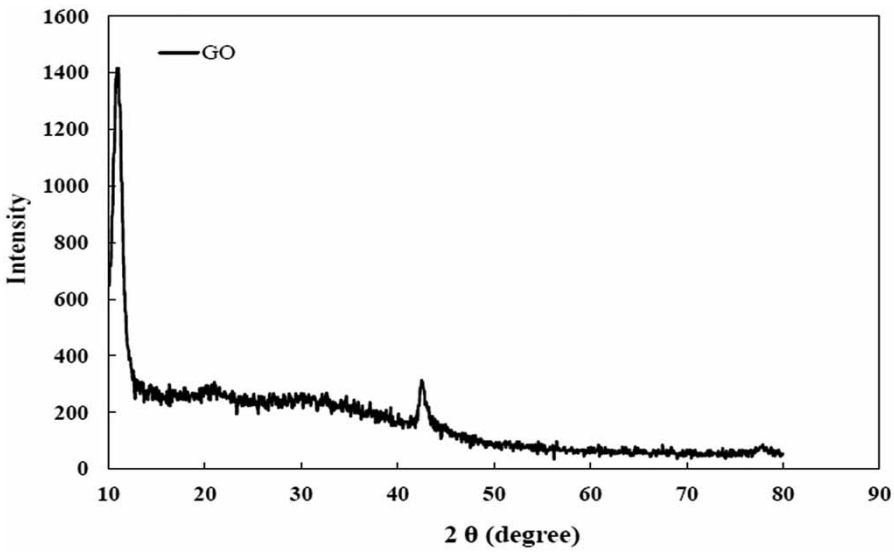

Figure 3 | XRD for graphene oxide.

(0.338 nm), it can be concluded that oxygen-based functional groups are formed on the surface of graphite nanosheets, and therefore, the distance between the plates increased (Li *et al.* 2015).

Evaluation of the capability of the modified electro-activated persulfate process

Figure 4 compares the results of the modified electro-persulfate process using graphene oxide nanoparticles under the optimal conditions obtained in the electro-persulfate process.

As can be seen, dye removal efficiency using the modified electro-persulfate system is 95% in 40 min and 98% in 60 min. While, dye removal efficiency using the electro-persulfate process is 88% in 40 min and 95% in 60 min, which indicates the improvement of the electro-persulfate system using graphene oxide nanoparticles.

Since the modified electro-persulfate system showed good performance in removing the dye, the higher concentrations of dye were investigated. The results of the dye removal efficiency at different dye concentrations and energy consumption are presented in Figure 5(a) and 5(b).

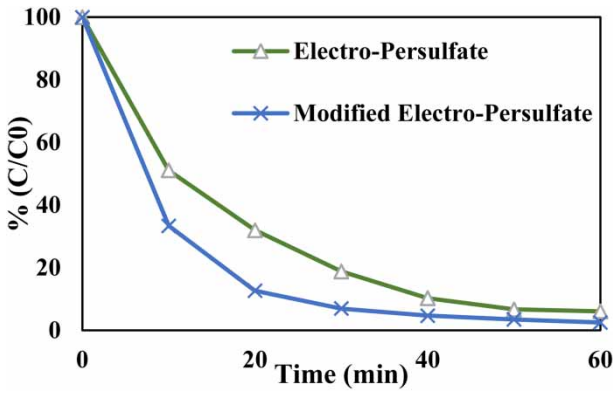

Figure 4 | Comparison of electro-persulfate process and modified electro-persulfate process. ([Dye] = 200 mg/L, pH = 5, [$Na_2S_2O_8$] = 500 mg/L, [$FeSO_4$] = 100 mg/L, I = 0.5 A, d = 2 cm.)

According to Figure 5(a), the dye removal efficiency after 60 min at dye concentrations of 200, 250, 300, and 350 mg/L is 98, 93, 90, and 80%, respectively. Figure 5(b) also shows that by increasing dye concentration, the amount of energy consumed to achieve removal efficiency of 90% (12–18 kg/kWh) has also increased. However, due to the negligible difference between the consumed energies, the dye concentration of 300 mg/L was selected as the optimal value in the modified electro-persulfate system. Comparing data extracting from the Table 1 and Figure 5, it can be seen that using graphene oxide nanoparticles has improved the capability of the electro-persulfate system and removed a higher concentration of dye. In the electro-persulfate system, 85% and 75% of dye concentrations of 200 and 250 mg/L were removed for 60 min, respectively. However, in the modified electro-persulfate system, the mentioned dye concentrations were removed by 98% and 93% after 60 min. Also, the energy consumption of the system at concentrations of 200 and 250 mg/L for 60 min in the electro-persulfate system was about 20–40 kWh/kg. Meanwhile, this parameter decreased to about 10–20 kWh/kg in the modified electro-persulfate system, which is due to graphene oxide nanoparticles that accelerated the electric current.

COMPARISON OF PROCESSES' KINETIC

In order to investigate the process kinetics, zero-order, pseudo-first-order, and pseudo-second-order kinetic models were used, and the best model was selected through the highest regression coefficient (R^2). Based on the results, both modified electro-persulfate and electro-persulfate processes follow first-order kinetics, the velocity constants of which are presented in Table 2. As can be seen, the modification of the electrodes in the electro-persulfate system has increased the reaction rate by about 17%, which shows its

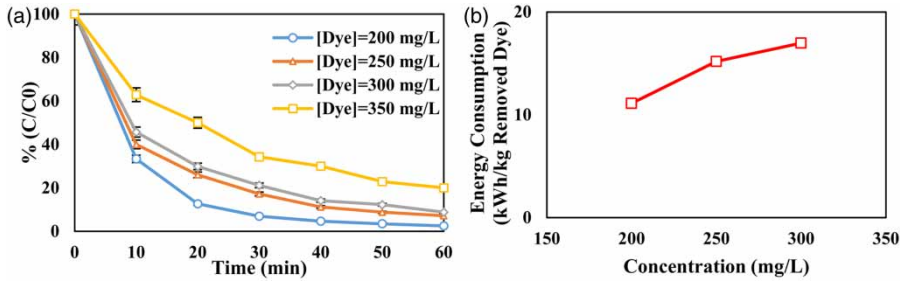

Figure 5 | (a) Effect of dye concentration on dye removal efficiency, and (b) effect of initial dye concentration on energy consumption in 90% dye removal efficiency. ([$Na_2S_2O_8$] = 500 mg/L, pH = 5, [$FeSO_4$] = 100 mg/L, I = 0.5 A, d = 2 cm.)

Table 2 | Velocity constants and regression coefficients of investigated processes in dye concentration of 200 mg/L

Process	Velocity constant	(R^2)
Electro-persulfate	0.0487	0.9892
Modified electro-persulfate	0.0592	0.9857

positive effect on system efficiency. This might be due to the positive impact of graphene oxide nanoparticles in accelerating the electric current and thus increasing the speed of the relevant reactions.

COD AND TOC REMOVAL IN MODIFIED ELECTRO-ACTIVATED PERSULFATE PROCESS

Although the reduction in the dye concentration is an essential parameter in the dye removal from aqueous solutions, it does not indicate the complete decomposition of the contaminant. In order to ensure the mineralization capability of the electrochemical process and its effect on the structure of the dye constituents, COD and TOC removal of the dye, dye adsorption spectra, and mean oxidation state were investigated in the modified electro-persulfate system under optimal conditions. It should be noted that since the time for dye removal was 60 min, a longer time (180 min) was chosen to remove the COD and TOC.

As can be seen in Figure 6(a), due to the ring structure and degradability of Acid Blue 25, COD removal (%) increased first due to the breakage of simpler bonds and benzene rings, and then had a fluctuation (Ghalebizade & Ayati 2019). Finally, after 180 min, 80% of the initial COD (254 mg/L COD for 300 mg/L dye concentration) decreased to 49 mg/L. According to Figure 6(b), the dye absorption spectra before the start of the reaction has two peaks in the wavelengths of 602 nm (anthraquinone group) and 361 nm (naphthalene ring) (Duman *et al.* 2011). The anthraquinone group is the coloring agent of Acid Blue 25, which significantly decreased during the reaction time. Comparing Figure 6(a) and 6(b), it can be seen that until 40 min, the COD removal (%) increases, and the dye adsorption decreases. But between 40 and 60 min, despite the decrease in COD removal percentage, the amount of dye absorption did not change significantly. These results indicate that despite the about 90% dye removal in 60 min, the complete mineralization of dye did not happen, and more time should be dedicated to discharge into the receiving environment. According to Figure 6(a), the TOC for the 300 mg/L dye concentration (65 mg/L TOC) also decreased by 54% after 180 min and reached 30 mg/L. In other words, the ratio of COD to TOC decreased from 3.84 to 1.63 after this period, which indicates the ability of the electro-persulfate process to break down the complex structure of Acid Blue 25 by sulfate radical and convert it into simpler compounds with less toxicity (Ghalebizade & Ayati 2016; Ghalebizade & Ayati 2019). According to Figure 7, after 40 min, the OX value increased from −6 to −4 ($OX_{methane} = -4$), after 80 and 120 min, it reached −2 ($OX_{benzene} = -2$) and 0 ($OX_{formaldehyde} = 0$), respectively, and after 180 min, it reached 2, which shows the formation of acidic compounds such as fumaric acid (OX = 2) due to the presence of strong oxidants such as persulfate and various radicals produced by the reduction of persulfate in the cathode electrode (Ghalebizade & Ayati 2020).

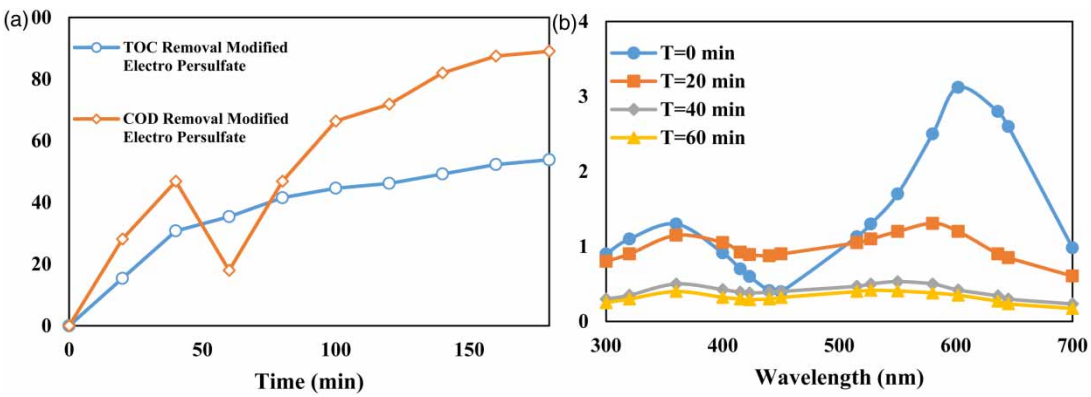

Figure 6 | (a) COD and TOC removal efficiencies, (b) dye absorption spectra, and ($[Na_2S_2O_8] = 500$ mg/L, pH = 5, $[FeSO_4] = 100$ mg/L, I = 0.5 A, d = 2 cm).

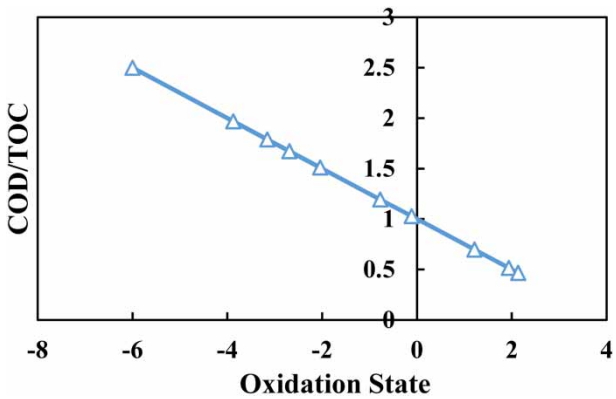

Figure 7 | Oxidation state changes in modified electro-persulfate process. ($[Na_2S_2O_8] = 500$ mg/L, pH = 5, $[FeSO_4] = 100$ mg/L, I = 0.5 A, d = 2 cm.)

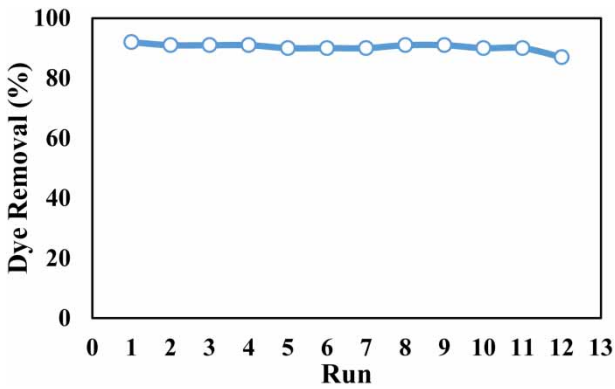

Figure 8 | Stability of graphene oxide nanoparticles on graphene electrodes. ($[Na_2S_2O_8] = 500$ mg/L, pH = 5, $[FeSO_4] = 100$ mg/L, I = 0.5 A, d = 2 cm.)

Stability of coated electrodes by graphene oxide nanoparticles

In order to confirm the use of graphene oxide nanoparticles coated on the graphite electrode, the experiments using the modified electro-persulfate process were repeated under optimal conditions, and dye removal efficiency was recorded, the results of which are presented in Figure 8.

The results show that after 11 tests, the dye removal efficiency was about 90% in 60 min and did not decrease significantly, which indicates the acceptable stability of the coating of graphene oxide nanoparticles on the graphite electrode. Rezaei Kalantari *et al.* (2018) also used Fe_3O_4 nanoparticles as a catalyst to remove amoxicillin in the electro-Fenton process, and based on the results, after eight tests, the removal efficiency decreased by 10% (Rezaei *et al.* 2018).

COMPARISON OF DIFFERENT ELECTRO-ACTIVATION SULFATE-BASED RADICALS

In this section, a comparison between the proposed graphene-oxide electrodes and other materials that have been widely used for sulfate-based radicals' generation is shown. One important factor in the electro-activated persulfate system is the amount of energy consuming in this process. Table 3 shows a comparison between energy comparison of the current work and other researches related to persulfate radicals' generation.

The comparison between graphene oxide electro-activated sulfate-based radicals and other carbon-based materials is depicted in Table 4. As can be seen, applying graphene oxide shows a great performance in the degradation of recalcitrant dye compound compared to other studies relating to TOC removal efficiency. The TOC removal in the current study was the same as that of Liu *et al.* (2018a, 2018b), but showed very fast kinetic in less time. Electro-activated sulfate-based using nano graphene oxide electrodes also had better performance in the

Table 3 | Comparison between different sulfate-based treatment systems from energy consumption aspect

Process	Pollutant	Concentration (mg/L)	Removal efficiency	Energy consumption (kWh/kg)	References
Electro-activated persulfate by graphene oxide	Acid blue 25	300	54% TOC	20	Current study
Electro/Fe^{2+}/persulfate	Bisphenol A	0.14 mM	61.8% TOC	253.9	Dos Santos *et al.* (2021)
Electro-activated persulfate by BDD anode	Malachite green	200	55% TOC	450 kWh/m^3	Miao *et al.* (2020)
Electro-activated persulfate by Iron electrodes	Ciprofloxacin	10	94%	0.0045 Wh/mg	Malakootian & Ahmadian (2019)
Sequential Persulfate/Fenton oxidation	Leachate	5,600 mg/L TOC	53% TOC	154	Silveira *et al.* (2018)

Table 4 | Comparison between graphene oxide electro-activated sulfate-based radicals and other carbon-based materials

Process	Pollutant	Pollutant concentration (mg/L)	Sulfate source concentration (mg/L)	Time (min)	K_{app} (1/min)	Removal efficiency	Reference
Electro-activated persulfate by graphene oxide	Acid blue 25	300	500 PMS	40	0.0592	54% TOC	Current study
Electro-activated carbon fiber peroxydisulfate	Carbamazepine	0.042 mM	100 mM PDS	120	0.0727	57% TOC	Liu *et al.* (2018a, 2018b)
Electro-activated graphite peroxydisulfate	Sulfamethoxazole	–	1000 mg/L PDS	5	0.9944	95%	Song *et al.* (2018)
Electro-activated graphite peroxydisulfate	Nitrobenzene	–	1000 mg/L PDS	30	0.0313	60%	Song *et al.* (2018)
Electro-activated graphite peroxydisulfate	Atrazine	–	1000 mg/L PDS	30	0.0415	75%	Song *et al.* (2018)
Electro-activated MWCNT peroxydisulfate	Sulfamethoxazole	–	1000 mg/L PDS	5	0.4568	80%	Song *et al.* (2018)

degradation of both nitrobenzene and atrazine pollutants. Therefore, this research indicates that graphene oxide can improve the performance of the electro-activated sulfate radical, promoting the pollutant decontamination.

CONCLUSIONS

Dyes have adverse effects on the environment due to their diverse chemical structure and non-biodegradability. Recently, persulfate ion as a strong oxidant compared to the others, Fe^{2+} ion as a strong catalyst and a cost-effective compound, and electrochemical processes as an environmentally friendly technology have attracted a lot of attention. However, the relatively low rate of electrochemical reactions prevents optimal removal efficiency. For this purpose, this study aimed to improve the electro-activated persulfate process for Acid Blue 25 removal from aqueous solutions by using graphene oxide nanoparticles, which is known as the catalyst and accelerator of electric current. According to the results, the use of graphene oxide nanoparticles reduced the reaction time from 60 to 40 min. It also increased the system capacity to remove a higher dye concentration from 200 to 300 mg/L.

ACKNOWLEDGEMENTS

The authors would like to thank Mr Behnam Nayebi, the Graduated MSc in Environmental Engineering from Civil & Environmental Engineering Faculty of Tarbiat Modares University for his great contribution in review and editing the paper.

DATA AVAILABILITY STATEMENT

All relevant data are included in the paper or its Supplementary Information.

REFERENCES

APHA-AWWA-WEF 2017 *Standard Methods for the Examination of Water and Wastewater*, 23rd edn. American Public Health Association/American Water Works Association/Water Environment Federation, Washington, DC, USA.

Asadi, A. & Mehrvar, M. 2006 Degradation of aqueous methyl tert-butyl ether by photochemical, biological, and their combined processes. *International Journal of Photoenergy* **2006**, 1–7.

Cai, J., Zhou, M., Liu, Y., Savall, A. & Serrano, K. G. 2018 Indirect electrochemical oxidation of 2, 4-dichlorophenoxyacetic acid using electrochemically-generated persulfate. *Chemosphere* **204**, 163–169.

Cai, W. W., Zhu, Y. W., Li, X. S., Piner, R. D. & Ruoff, R. S. 2009 Large area few-layer graphene/graphite films as transparent thin conducting electrodes. *Journal of Applied Physics* **95**, 115–123.

Devi, P., Das, U. & Dalai, A. K. 2016 In-situ chemical oxidation: principle and applications of peroxide and persulfate treatments in wastewater systems. *Science of The Total Environment* **571**, 643–657.

Dos Santos, A. J., Sirés, I. & Brillas, E. 2021 Removal of bisphenol A from acidic sulfate medium and urban wastewater using persulfate activated with electroregenerated Fe^{2+}. *Chemosphere* **263**, 128271.

Duman, O., Tunc, S. & Kanci, B. 2011 Spectrophotometric studies on the interactions of C.I. Basic Red 9 and C.I. Acid Blue 25 with hexadecyltrimethylammonium bromide in cationic surfactant micelles. *Fluid Phase Equilibria* **301**, 56–61.

Eckenfelder Jr, W. 1999 *Industrial Water Pollution Control*, 3rd edn. McGraw-Hill Science, Boston, MA, USA.

Ghalebizade, M. & Ayati, B. 2016 Solar photoelectrocatalytic degradation of Acid Orange 7 with ZnO/TiO_2 nanocomposite coated on stainless steel electrode. *Process Safety and Environment Protection* **103**, 192–202.

Ghalebizade, M. & Ayati, B. 2019 Acid Orange 7 treatment and fate by electro-peroxone process using novel electrode arrangement. *Chemosphere* **235**, 1007–1014.

Ghalebizade, M. & Ayati, B. 2020 Investigating electrode arrangement and anode role on dye removal efficiency of electro-peroxone as an environmental friendly technology. *Seperation and Purification Technology* **251**, 1383–5866.

Gholami, A., Bahrami, A., Arami, H. & Pajootan, M. 2017 Photocatalytic dye removal using GO-TiO_2 modified electrode and optimization by RSM. *Journal of Color Science and Technology* **11** (3), 187–202.

Hassan, H. & Hameed, B. H. 2011 Decolorization of Acid Red 1 by heterogeneous Fenton-like reaction using Fe-ball clay catalyst. In: *International Conference on Environment Science and Engineering IPCBEE IACSIT Press Singapore*.

Idel-aouad, R., Valiente, M., Yaacoubi, A., Tanouti, B. & López-Mesas, M. 2011 Rapid decolourization and mineralization of the azo dye CI Acid Red 14 by heterogeneous Fenton reaction. *Journal of Hazardous Materials* **186**, 745–750.

Ike, I. A., Linden, K., Orbell, J. D. & Duke, M. 2018 Critical review of the science and sustainability of persulfate advanced oxidation processes. *Chemical Engineering Journal* **338**, 651–669.

Jiang, X., Wu, Y., Wang, P., Li, H. & Dong, W. 2013 Degradation of bisphenol A in aqueous solution by persulfate activated with ferrous ion. *Environmental Science and Pollution Research* **20** (7), 4947–4953.

Kansal, S. K., Ali, A. H. & Kapoor, S. J. D. 2010 Photocatalytic decolorization of biebrich scarlet dye in aqueous phase using different nanophotocatalysts. *Desalination* **259** (1–3), 147–155.

Khataee, A., Akbarpur, A. & Vahid, B. 2013 Photoassisted electrochemical degradation of an azo dye using Ti/RuO_2 anode and carbon nanotubes containing gas-diffusion cathode. *Journal of the Taiwan of Chemical Engineers* **727**, 1–7.

Kim, J., Cote, L. J., Kim, F., Yuan, W., Shull, K. R. & Huang, J. X. 2006 Graphene oxide sheets at interfaces. *Journal of American Chemical Society* **132**, 8180–8186.

Li, X. S., Zhu, Y. W., Cai, W. W., Borysiak, M., Han, B. Y., Chen, D., Piner, R. D., Colombo, L. & Ruoff, R. S. 2009 Transfer of large-area graphene films for high performance transparent conductive electrodes. *Nano Letters* **9** (12), 4359–4363.

Li, X. H., Feng, J., Du, Y. P., Bai, J. T., Fan, H. M. & Zhang, H. L. 2015 One-pot synthesis of $CoFe_2O_4$/graphene oxide hybrids and their conversion into FeCo/graphene hybrids for lightweight and highly efficient microwave absorber. *Journal of Materials Chemistry A* **3** (10), 5535–5546.

Li, J., Ren, Y., Lai, L. & Lai, B. J. 2018 Electrolysis assisted persulfate with annular iron sheet as anode for the enhanced degradation of 2, 4-dinitrophenol in aqueous solution. *Journal of Hazardous Materials* **344**, 778–787.

Lin, H., Wu, J. & Zhang, P. 2013 Degradation of bisphenol A in aqueous solution by a novel electro/Fe^{3+}/peroxydisulfate process. *Separation and Purification Technology* **117**, 18–23.

Lin, H., Zhang, H. & Hou, L. 2014 Degradation of C.I. Acid Orange 7 in aqueous solution by a novel electro/Fe_3O_4/PDS process. *Journal of Hazardous Materials* **276**, 182–191.

Liu, J., Zhong, S., Song, Y., Wang, B. & Zhang, F. J. 2018a Degradation of tetracycline hydrochloride by electro-activated persulfate oxidation. *Journal of Electroanalytical Chemistry* **809**, 74–79.

Liu, Z., Zhao, C., Wang, P., Zheng, H., Sun, Y. & Dionysiou, D. D. 2018b Removal of carbamazepine in water by electro-activated carbon fiber-peroxydisulfate: comparison, optimization, recycle, and mechanism study. *Chemical Engineering Journal* **343**, 28–36.

Lu, W., Chen, J., Wu, Y., Duan, L., Yang, Y. & Xin, G. 2014 Graphene-enhanced visible-light photocatalysis of large-sized CdS particles for wastewater treatment. *Nanoscale Research Letters* **148**, 1–7.

Malakootian, M. & Ahmadian, M. 2019 Ciprofloxacin removal by electro-activated persulfate in aqueous solution using iron electrodes. *Applied Water Science* **9** (5), 1–10.

Masomboon, N., Ratanatamskul, C. & Lu, M. C. 2010 Chemical oxidation of 2, 6-dimethylaniline by electrochemically generated fenton's reagent. *Journal of Hazardous Material* **176** (1–3), 92–98.

Miao, D., Liu, G., Wei, Q., Hu, N., Zheng, K., Zhu, C., Liu, T., Zhou, K., Yu, Z. & Ma, L. 2020 Electro-activated persulfate oxidation of malachite green by boron-doped diamond (BDD) anode: effect of degradation process parameters. *Water Science and Technology* **81** (5), 925–935.

Nayebi, B. & Ayati, B. 2021 Degradation of emerging amoxicillin compound from water using the electro-Fenton process with an aluminum anode. *Water Conservation Science and Engineering* **6**, 45–54.

Panda, N., Sahoo, H. & Mohapatra, S. 2011 Decolourization of Methyl Orange using Fenton-like mesoporous Fe_2O_3-SiO_2 composite. *Journal of Hazardous Materials* **185**, 359–365.

Phalakornkule, C., Polgumhang, S., Tongdaung, W., Karakat, B. & Nuyut, T. 2010 Electrocoagulation of blue reactive, red disperse and mixed dyes, and application in treating textile effluent. *Journal of Environmental Management* **91** (4), 918–926.

Rastogi, A., Al-Abed, S. R. & Dionysiou, D. D. 2009 Sulfate radical-based ferrous-PMS oxidative system for PCBs degradation in aqueous and ediment systems. *Applied Catalysis B Environmental* **85**, 171–179.

Rezaei Kalantary, R., Farzadkia, M., Kermani, M. & Rahmatinia, M. 2018 Heterogeneous electro-Fenton process by Nano-Fe_3O_4 for catalytic degradation of amoxicillin: process

optimization using response surface methodology. *Journal of Environmental Chemical Engineering* **6** (4), 4644–4652.

Robinson, T., McMullan, G., Marchant, R. & Nigam, P. 2001 Remediation of dyes in textile effluent: a critical review on current treatment technologies with a proposed alternative. *Bioresource Technology* **77** (3), 247–255.

Silveira, J. E., Garcia-Costa, A. L., Cardoso, T. O., Zazo, J. A. & Casas, J. A. 2017 Indirect decolorization of azo dye Disperse Blue 3 by electro-activated persulfate. *Electrochimica Acta* **258**, 927–932.

Silveira, J. E., Zazo, J. A., Pliego, G. & Casas, J. A. 2018 Landfill leachate treatment by sequential combination of activated persulfate and Fenton oxidation. *Waste Management* **81**, 220–225.

Song, H., Yan, L., Jiang, J., Ma, J., Pang, S., Zhai, X., Zhang, W. & Li, D. 2018 Enhanced degradation of antibiotic sulfamethoxazole by electrochemical activation of PDS using carbon anodes. *Chemical Engineering Journal* **344**, 12–20.

Szabo, T., Tombacz, E., Illes, E. & Dekany, I. 2006 Enhanced acidity and pH-dependentsurface charge characterization of successively oxidized graphite oxides. *Carbon* **44**, 537–545.

Wacławek, S., Lutze, H. V., Grübel, K., Padil, V. V., Černík, M. & Dionysiou, D. D. 2017 Chemistry of persulfates in water and wastewater treatment: a review. *Chemical Engineering Journal* **330**, 44–62.

Wang, J. & Wang, S. 2018 Activation of persulfate (PS) and peroxymonosulfate (PMS) and application for the degradation of emerging contaminants. *Chemical Engineering Journal* **334**, 1502–1517.

Yuan, S., Liao, P. & Alshawabkeh, A. N. 2013 Electrolytic manipulation of persulfate reactivity by iron electrodes for trichloroethylene degradation in groundwater. *Journal of Environmental Science and Technology* **48** (1), 656–663.

Zaaba, N. I., Foo, K. L., Hashim, U., Tan, S. J., Liu, W. W. & Voon, C. H. 2017 Synthesis of graphene oxid using modified hummers method: solvent influence. *Procedia Engineering* **184**, 469–477.

Zahraa, O., Maire, S., Evenou, F., Hachem, C., Pons, M. N., Alinsafi, A. & Bouchy, M. 2006 Treatment of wastewater dyeing agent by photocatalytic process in solar reactor. *International Journal of Photoenergy* **2006**, 1–9.

Zazouli, M. A. & Taghavi, M. 2012 Phenol removal from aquous solutions by electrocoagulation technology using iron electrodes: effect of some variables. *Journal of Water Resource and Protection* **4** (11), 980–983.

Zhang, H., Honglu, Z., Aldalbahi, A., Zuo, X., Fan, C. & Mi, X. 2017 Fluorescent biosensors enabled by graphene and graphene oxide. *Biosensors and Bioelectronics* **89**, 96–106.

Zhou, L., Zheng, W., Ji, Y., Zhang, J., Zeng, C., Zhang, Y., Wang, Q. & Yang, X. 2013 Ferrous-activated persulfate oxidation of arsenic (III) and diuron in aquatic system. *Journal of Hazardous Materials* **263**, 422–430.

Zou, J., Ma, J., Chen, L., Li, X., Guan, Y., Xie, P. & Pan, C. 2013 Rapid acceleration of ferrous iron/peroxymonosulfate oxidation of organic pollutants by promoting Fe (III)/Fe (II) cycle with hydroxylamine. *Enivironmental Science and Technology* **47** (20), 11685–11691.

First received 21 January 2021; accepted in revised form 23 March 2021. Available online 2 April 2021